HHS Public Access

Author manuscript

J Proteome Res. Author manuscript; available in PMC 2015 June 04.

Published in final edited form as:

J Proteome Res. 2015 May 1; 14(5): 2109–2120. doi:10.1021/pr501238m.

Proteomic Profiling of the Retinas in a Neonatal Rat Model of Oxygen-Induced Retinopathy with a Reproducible Ion-Current-Based MS1 Approach

Chengjian Tu[#*,†,‡], **Kay D. Beharry**[#§,∥,⊥], **Xiaomeng Shen**[†,‡], **Jun Li**[†,‡], **Lianshui Wang**[#], **Jacob V. Aranda**[§,∥,⊥], and **Jun Qu**[*,†,‡]

[†]Department of Pharmaceutical Sciences, University at Buffalo, State University of New York, Buffalo, New York 14260, United States

[‡]New York State Center of Excellence in Bioinformatics and Life Sciences, 701 Ellicott Street, Buffalo, New York 14203, United States

[§]Department of Pediatrics, Division of Neonatal-Perinatal Medicine, State University of New York, Downstate Medical Center, Brooklyn, New York 11203, United States

[∥]Department of Ophthalmology, State University of New York, Downstate Medical Center, Brooklyn, New York 11203, United States

[⊥]SUNY Eye Institute, Syracuse, New York 13202, United States

[#]The State Key Laboratory of Microbial Technology, Shandong University, Jinan, Shandong 250100, China

[#] These authors contributed equally to this work.

Abstract

Investigation of the retina proteome during hypoxia-induced retinal neovascularization is valuable for understanding pathogenesis of retinopathy of prematurity (ROP). Here we employed a reproducible ion-current-based MS1 quantification approach (ICB) to explore the retinal proteomic changes in early stage of ROP in a rat model of oxygen-induced retinopathy (OIR). Retina proteins, which are rich in membrane proteins, were efficiently extracted by a detergent-cocktail and subjected to precipitation/on-pellet-digestion, followed by nano-LC-MS analysis on a 75-cm column with a 7-h gradient. The high reproducibility of sample preparation and

Corresponding Authors[*] C.T.: Phone: (716) 888-4729. Fax: (716) 645-3693. ctu3@buffalo.edu. J.Q.: Phone: (716) 645-2844 x283. Fax: (716) 645-3693. junqu@buffalo.edu..

Supporting Information Supplemental Table 1: protein report file of each run from the retinas of OIR versus controls experiment (n = 4/group). Supplemental Table 2: quantitative information on 1325 proteins and associated peptides using ICB label-free quantification. Supplemental Figure 1: Evaluation of reproducibility for lower-abundance proteins between two technical replicates with different label-free approaches. Supplemental Figure 2: GO-cellular component annotation of the 1326 identified proteins identified from retinas of rats with OIR and age-matched controls. Supplemental Figure 3: Coefficients of variation of the abundance values of the 1325 proteins quantified by ICB (n = 4 LC-MS/MS analyses). Supplemental Figure 4: Peptide intensity distribution of radixin. Supplemental Figure 5: Distribution of peptide ratios derived from the elevated proteins (A) and decreased proteins (B) in retinas of OIR versus controls. Supplemental Figure 6: GO-biological process annotation of the 32 differentially expressed proteins from retinas of OIR vs age-matched control rats. This material is available free of charge via the Internet at http://pubs.acs.org.

The authors declare no competing financial interest.

chromatography separation enabled excellent peak alignment and contributed to the superior performance of ICB over parallel label-free approaches. In this study, sum-of-intensity with rejection was incorporated to determine the protein ratios. In total, 1325 unique protein groups were quantified from rat retinas (n = 4/group) with at least two distinct peptides at a protein FDR of 1%. Thirty-two significantly altered proteins were observed with confidence, and the elevated glial fibrillary acidic protein and decreased crystalline proteins in OIR retinas agree well with previous studies. Selected key alterations were further validated by Western blot analysis. Interestingly, Rab21/RhoA/ROCK2/moesin signaling pathway was found to be involved in retinal neovascularization of OIR. Moreover, highly elevated annexin A3, a potential angiogenic mediator, was observed in OIR retinas and may serve as a potential therapeutic target. In conclusion, reproducible ICB profiling enabled reliable discovery of many altered mediators and pathways in OIR retinas, thereby providing new insights into molecular mechanisms involved in pathogenesis of ROP.

Keywords

label-free quantification; *neovascularization*; *oxygen-induced retinopathy*; *peptide ion current areas*; *retinopathy of prematurity*

INTRODUCTION

Retinopathy of prematurity (ROP), a leading cause of blindness in childhood, is a vision disease associated with abnormal retinal vascular development in extremely low gestational age neonates.[1,2] For those premature infants, supplemental oxygen is routinely applied to maintain adequate blood oxygen levels, which greatly increases survival rate but also increases the number of infants with ROP.[3,4] Although surgical intervention such as laser photocoagulation or cryotherapy reduces the incidence of blindness, the visual outcomes after treatment often are poor.[5,6] Thus, preventive therapy of aberrant neovascularization for continued development of the normal intra-retinal vasculature is sorely needed. Recently the most popular targets for therapy are angiogenesis related factors such as vascular endothelial growth factor (VEGF), insulin-like growth factor, and the Src family of tyrosine kinases.[7–9] A deep understanding of the retina proteome changes during hypoxia-induced retinal neovascularization may be valuable in developing new therapeutic targets for newborns with ROP.

Due to the scarcity of human donor eyes of ROP, the rodent models of oxygen-induced retinopathy (OIR) are widely used to mimic ROP in humans.[10–12] Retinal oxygen supply and consumption in those animals are similar to that of primates, thus enabling the use of these models to study the hypoxia-induced retinal neovascularization.[13,14] To promote retinal neovascularization, neonatal rats or mice are usually first exposed to a constant high oxygen level (50%–80%) for more than 1 week.[15,16] The oxygen-enriched atmosphere mediates the inhibition of retinal vessel growth and also suppresses endogenous VEGF production.[15,16] After 5–7 days of recovery in room air, a relatively hypoxic environment, the angiogenic stimulators are produced, and thus retinal neovascularization is induced.[10,14]

Here we use a rat model of OIR to perform mechanism studies of ROP as previously described.[17]

Liquid chromatography–mass spectrometry (LC-MS)-based proteomic quantification plays a key role in discovering pathogenic factors and biomarkers of various diseases. Roughly, LC-MS-based relative protein quantitation can be divided into two major categories, labeling and label-free methods. While stable isotope labeling approaches have been tremendously successful and widely applied in quantitative proteomics, certain drawbacks do exist, such as expensive reagents, incomplete and variable labeling, limitation in sampling size, and, in some cases, complex data interpretation.[18,19] Label-free approaches have emerged as an attractive alternative to isotope-labeling methods, due to its simplicity, cost-effectiveness, and feasibility of quantifying multiple biological samples.[18,20,21] Especially, ion-current- or MS1-based strategies are capable of providing a reliable means for in-depth protein profiling and biomarker discovery in complex proteomes.[22–25] The superior performance of ion-current-based (ICB) method compared to other popular label-free approaches such as MS2-TIC and spectral counting, in terms of reproducibility, quantitative accuracy, dynamic range, and biomarker discovery, has been demonstrated when using high-resolution MS data.[22,26]

For retinal proteome analysis in a rodent model of OIR, the isobaric tags for relative and absolute quantification (iTRAQ) technique has been widely applied and enables researchers to quantify nearly 300 reliable proteins in previous studies.[27,28] In the current study, ICB approach coupled with long gradient nano-LC-MS/MS analysis is employed. Each step of the analytical procedures is carefully optimized and controlled to ensure optimal reproducibility and sensitivity. More than 1300 unique protein groups with at least two distinct peptides are quantified in retinas of rat samples (OIRs vs controls) under strict criteria. This is the first time that an extensive proteomic profiling analysis has been applied to study of pathological mechanisms of ROP in retina.

MATERIALS AND METHODS

All animal experiments were approved by the State University of New York, Downstate Medical Center Institutional Animal Care and Use Committee (Brooklyn, NY). Animals were managed according to the Association for Research in Vision and Ophthalmology Statement for the Use of Animals in Ophthalmic and Visual Research. Animals were treated humanely, according to the guidelines outlined by the United States Department of Agriculture and the Guide for the Care and Use of Laboratory Animals.

Rat Model of OIR

Pregnant Sprague–Dawley rats were purchased from Charles River Laboratories, Inc. (Wilmington, MA) at 17 days gestation. On the day of birth, newborn rat pups (n = 18 pups/group, 9 males and 9 females) delivering on the same day were randomly assigned to OIR or room air (RA, control). In this study only retinas from male rats (n = 4/group) were used for proteomic study. The OIR pups were placed with the dams in specialized oxygen chambers attached to an oxycycler (BioSpherix, New York) which is attached to oxygen chambers. The oxygen chamber was optimized for gas efficiency and provided adequate ventilation for the animals in a controlled atmosphere with minimal gas usage. Oxygen content inside the

chamber was continuously monitored and recorded on a Dell Computer. CO_2 and humidity inside the chamber were also continuously monitored, and CO_2 was removed from the atmosphere with the use of soda lime within the chamber. The pups in the experimental group were exposed to a 50% oxygen atmosphere for 14 days (P0–P14), followed by reoxygenation in RA for 7 days from P15–P21. Control littermates were raised in RA from birth to P21. All the rats were sacrificed at P21, and the eyes were enucleated and rinsed in ice-cold phosphate-buffered saline (pH 7.4) on ice. The retinas were then excised and processed as previously described.[12,29]

Retinal Protein Preparation and Precipitation/On-Pellet Digestion

Retinas from four male rats in each group were analyzed. The retinal protein extraction and subsequently tryptic digestion were processed as described.[22] Each isolated retina (n = 4 samples/group) was homogenized in 400 μL of ice-cold lysis buffer (50 mM Tris-formic acid, 150 mM NaCl, 0.5% sodium deoxycholate, 2% SDS, 2% NP-40, pH8.0) with a Polytron homogenizer (Kinematica AG, Switzerland). The tissue homogenization was performed for 5–10 s at 15 000 rpm, followed by a 20-s cooling period until the foam settled; then this procedure was repeated 10 times. The mixture was then sonicated in a cold room (4 °C) for ~10 min with a low-power bath sonicator. Subsequent centrifugation at 140000g was performed for 1 h at 4 °C, and the resulting supernatant was transferred to a new tube. The protein concentration was determined by bicinchoninic acid protein assay (Pierce Biotechnology, Inc.), and the remaining samples were stored at −80 °C until further analysis.

To achieve high peptide recovery, we employed a precipitation/on-pellet-digestion protocol modified from that described previously.[22,30] Briefly, specimens (100 μg of total protein per sample) were reduced with 3 mM tris(2-carboxyethyl)phosphine for 10 min and then alkylated with 20 mM iodoacetamide for 30 min in darkness. The mixture was transferred to acetone-compatible tube and precipitated by stepwise addition of 9 volumes of chilled acetone (−20 °C) with continuous vortexing. After overnight incubation at −20 °C, the protein mixture was centrifuged at 12000g for 20 min at 4 °C. The resulting supernatant was removed, and the remaining pellet was air-dried at room temperature. To improve tryptic digestion effciency, two-step digestion procedure was employed for the on-pellet-digestion. In step 1 (pellet-dissolving step), 50 μL of Tris buffer (50 mM, pH 8.5) containing trypsin at a ratio of 1:30 (enzyme/substrate) was added and incubated at 37 °C for 6 h with agitation at 500 rpm in an Eppendorf Thermomixer (Hamburg, Germany); in step 2 (complete-cleavage step), another 50 μL of trypsin solution was added at a ratio of 1:25, and the mixture was incubated at 37 °C overnight (12 h).

Nano-LC-MS/MS Analysis

In order to achieve low void volume and high chromatographic reproducibility during peptides separation, a nano-LC/nanospray setup was used as previously described.[30] Mobile phases A and B were 0.1% formic acid in 2% acetonitrile and 0.1% formic acid in 88% acetonitrile, respectively. The tryptic peptide mixture (4 μg) was loaded onto a large-inner-diameter trap (300 μm i.d. × 1 cm, packed with Zorbax 3-μm C18 material), and washed for 3 min with 1% mobile phase B at a flow rate of 10 μL/min. A series of nanoflow gradients

(flow rate, 250 nL/min) was used to back-flush the trapped samples onto the nano-LC column (75 μm i.d. × 75 cm, packed with Pepmap 3-μm C18 material) for separation. We steadily heated the nano-LC column at 52 °C to improve the chromatographic resolution and reproducibility. The complex peptide mixture was separated using a 7-h gradient, which consisted of the following steps: 3% B for 10 min, 3% to 8% B in 5 min, 8% to 24% B in 145 min, 24% to 38% B over 95 min, 38% to 63% B over 55 min, 63% to 97% B in 35 min, then maintaining isocratic conditions at 97% B for 25 min, and finally reverting back to 3% B for 40 min of re-equilibration.

An LTQ/Orbitrap XL-ETD hybrid mass spectrometer (Thermo Fisher Scientific, San Jose, CA) was used for protein identification. The instrument was operated in positive ion mode with the data-dependent acquisition strategy. One scan cycle included an MS1 scan (*m*/*z* 310–1800) at a resolution of 60 000, followed by seven MS2 scans in collision-induced dissociation activation mode, to fragment the seven most abundant precursors found in the MS1 spectrum. The respective target values for MS1 by Orbitrap and MS2 by ion trap were 6×10^6 and 1×10^4. The maximum ion times for Orbitrap and ion trap were 1300 and 150 ms, respectively. The activation time was 30 ms, the isolation width was 3 Da for the linear ion trap (LTQ), the normalized activation energy was 35%, and the activation *q* was 0.25. The dynamic exclusion was enabled with the following settings: repeat count, 1; repeat duration, 30 s; exclusion list size, 500; exclusion duration, 40 s. In this study, four respective retinas of experimental group (OIR) and control group were analyzed alternatively.

Protein Identification and Ion-Current-Based Quantification

The raw data files were processed and searched against the Swiss-Prot protein database (released November 2011), under rat and mouse taxonomy with a total of 16 071 protein entries, using the Proteome Discoverer 1.4 (Thermo-Scientific, San Jose, CA). The following search parameters were used: 20 ppm tolerance for precursor ion masses and 0.5 Da for fragment ion masses. Two missed cleavages were permitted for fully tryptic peptides. Carbamidomethylation of cysteines was set as a fixed modification, and a variable modification of methionine oxidation was allowed. The false discovery rate (FDR) was detected by using a target-decoy search strategy.[31] The sequence database contained each sequence in both forward and reversed orientations, enabling FDR estimation. Scaffold 3.6[32] (Proteome Software, Portland, OR) was used to validate MS/MS-based peptide and protein identification on the basis of cross-correlation (Xcorr) and Delta Cn values. The peptide filtering criteria include Delta Cn scores of ≥0.1 and Xcorr scores of ≥1.95, 2.40, 2.55, and 2.95, respectively, for singly, doubly, triply, and quadruply charged peptides. Along with the requirement of at least two distinct peptides for each protein group, a low FDR of 0.1% and 1.0% were achieved at the peptide level and protein level, respectively.

ICB quantitative analysis was performed using SIEVE v2.0 software (Thermo Scientific) to obtain area-under-the-curve (AUC) data and then a sum-intensity method coupled with outlier analysis to aggregate the quantitative data from peptide level to protein level. SIEVE is a MS1-based differential expression package that includes chromatographic alignment and global MS1 feature extraction.[33] Quantitative MS1 features (frames) were defined on the basis of *m*/*z* (width: 10 ppm) and retention time (width: 2.5 min) in the aligned collective

data set. Peak AUC values were calculated in each frame. In case of missing data, a value of 1000 was assigned at peptide level as previously demonstrated.[26] Subsequent to relative quantification, MS2 fragmentation scans associated with each frame were determined on the basis of identification results from Scaffold by using tools in-house as previously described.[34] Peptides shared among different protein groups were excluded from quantitative analysis. The ion current values of each peptide were normalized by the total AUC in individual runs. Intensities for unique peptides of the same protein were further combined to be the protein intensity with Grubbs's test[35] analysis by the ListPOR (version 2.2.2104) program (panomics.pnnl.gov). Minimum data set presence 2 and *p*-value cutoff of 0.01 were set for outlier detection. The relative expression ratio was calculated by the average ion-current intensities of four replicates in each group. Statistical significance between groups (comparing treated vs control specimens) was evaluated using a Student's *t*-test, and a *p*-value cutoff of 0.05 was applied.

We further compared the reproducibility of six popular label-free approaches: spectral counting (SpC), ion-current-based method (ICB), MS2 total-ion-current (MS2-TIC), TOP3 TIC,[36] exponentially modified protein abundance index (emPAI),[37] and the normalized spectral abundance factor (NSAF)[38] between technical replicates of a retina sample of rat. Except ICB, the other five methods were applied to analyze these two replicates using Scaffold 3.6. The abundance values of each protein were normalized by the total abundance values in individual runs.

Western Blot Analyses

For Western blot analyses, retina protein samples (25 μg each) in lysis buffer (50 mM Tris-formic acid, 150 mM NaCl, 0.5% sodium deoxycholate, 2% SDS, 2% NP-40, pH8.0) were first separated by SDS-PAGE using standard methodology with 10% polyacrylamide gels (Invitrogen). Proteins then were electrophoretically transferred to polyvinylidene difluoride membranes (Invitrogen). The membrane was blocked for 1 h with Western blocking solution (Invitrogen) and sequentially incubated with a primary antibody overnight at 4 °C followed by an appropriate secondary antibody conjugated with horseradish peroxidase (Santa Cruz Biotechnology, Inc., Dallas, TX) for 1 h. The positive immunoreactions were detected with X-ray film by chemiluminescence using an ECL Western blotting kit (Pierce, Rockford, IL) and developed with a Kodak X-OMAT 2000A Processor. The primary antibodies used in this study were as follows: mouse monoclonal anti-GFAP (1:400; SigmaAldrich); rabbit polyclonal anti-signal transducer and activator of transcription 1 (Stat1 p84/p91) (1:500; Santa Cruz Biotechnology); and mouse monoclonal anti-glyceraldehyde-3-phosphate dehydrogenase (GAPDH) (1:1000; Santa Cruz Biotechnology).

Bioinformatics Analysis

Protein function annotation and pathway analysis were carried out using Ingenuity Pathway Analysis (IPA, Ingenuity Systems, http://www.ingenuity.com/). Ingenuity's knowledge base is created by manual curation of the scientific literature supported by experimental results. The altered protein list was imported directly into IPA for a Core analysis. Biological functions assigned by the software were manually examined and regrouped into respective categories. Gene ontology (GO) annotations were analyzed with online DAVID

Bioinformatics Resources 6.7 tool.[39] Hierarchical cluster analysis was performed using Cluster 3.0[40] and displayed by TreeView (Java software), which supports tree-based and image-based browsing of hierarchical trees (http://www.eisenlab.org). In the heat map generated by TreeView, the elevated protein intensities are indicated in red, and the decreased protein intensities are indicated in green.

RESULTS AND DISCUSSION

A rat model of OIR was employed to investigate the molecular mechanism of ROP using ICB profiling approach. Though the newborn rats are not premature, they have incompletely vascularized retinas at birth, thus making them susceptible to development of characteristics consistent with severe ROP or OIR. The rat model shares many similar clinicopathological features with the human disease counterpart, including preretinal neovascularization, vitreal hemorrhage, arteriovenous shunts, frequent retinal folds, and occasional retinal detachment.[14,41] Therefore, most rodent models of ROP use newborn, full term animals exposed to constant high levels of inspired oxygen followed by RA.[10–12,14] In the rat model of OIR used in this study, retinal neovascularization and accumulation of retinal hydrogen peroxide (H_2O_2) level were observed, as demonstrated in recent studies.[17] To achieve a reliable discovery of altered proteins in retinas that are rich in membrane proteins, we have developed a reproducible, extensive, and well-controlled strategy for the profiling of the retinal proteome with multiple biological replicates as we previously reported.[22] Here we employed a similar strategy to perform proteomic profiling of the retinas in a neonatal rat model of OIR. The flowchart of ICB quantitative approach was shown in Figure 1. A strong buffer containing a cocktail of detergents (2% NP-40, 2% SDS, and 0.5% sodium deoxycholate) was used to efficiently extract proteins from retinas. The extracted proteins were processed with a reproducible precipitation/on-pellet-digestion procedure to remove detergents and other contaminants and then efficiently digest the extracts. The resulting peptide mixture was further separated with a low-void-volume nano-LC/nanospray configuration providing improved peak shapes, reduced tailing, and high run-to-run reproducibility. Finally, the multiple LC-MS runs were analyzed by the ICB quantification, and significantly altered proteins were validated and annotated.

Evaluation of Reproducibility of Different Label-Free Approaches

High quantitative reproducibility is critically important for label-free methods. It has been shown that ICB method exhibited an overall superior performance than SpC and MS2-TIC methods in terms of reproducibility, missing data, and biomarker discovery for analyzing high-resolution MS data as we previously described.[22,26] Besides ICB, MS2-TIC, and SpC, here we also evaluated the reproducibility of another three popular label-free abundance approaches: TOP3 TIC,[36] emPAI,[37] and the NSAF[38] between two technical replicates. A total of 1239 protein groups (protein FDR of 1%) were identified from two consecutive replicate LC-MS analyses of a rat retina sample. In case of missing data in any of methods, a value of zero was assigned to the affected replicate. Normalization was performed against the sum of individual abundance values in each replicate.

For ICB, all 1239 proteins were quantified without missing value while for the MS2-based methods only 1170 (94%) proteins with quantitative values in both technical replicates were

analyzed. Linear regression analysis was performed by GraphPad Prism (GraphPad Software, Inc., USA) to assess the correlation between replicate runs using each of the quantitative methods. We separated the quantifiable proteins by each method into two groups: high-abundance proteins (the top 50% abundant proteins as determined by individual quantitative values) and lower-abundance proteins (the remaining 50% proteins). The results for lower-abundance proteins (i.e., the lower 50% of all proteins) are shown in Figure 2. A higher R^2 value (0.96) was achieved by ICB method than all other methods, indicating much better reproducibility. By comparison, all methods showed good reproducibility (R^2>0.95) for higher abundance proteins (Supplemental Figure 1), which is in line with our previous reports.[23,26,42,43] As a result, in this study the ICB was employed to investigate the molecular mechanism of OIR.

Proteomic Profiling of Retinas in OIR Rats

In the OIR/control sample set, a total of 1339 protein groups (including 13 decoy proteins) with at least two distinct peptides each were identified with a low FDR of 1% at protein level. The detailed protein identification data are listed in Supplemental Table 1. The numbers of proteins analyzed here is much higher than that from the iTRAQ experiments of OIR models reported previously.[27,28] GO annotations were analyzed with online DAVID Bioinformatics Resources 6.7 tool.[39] Among the 1231 proteins with available GO cellular component information, 371 (30.1%), 329 (26.7%), and 273 (22.2%) were respectively assigned as membrane, nucleus, and cytosol proteins as shown in Supplemental Figure 2, indicating high recovery of membrane proteins by the sample preparation strategy. As the retina is part of the central nervous system, 66 proteins attributed to synapse were observed (Supplemental Figure 2).

We performed an extensive quantitative comparison of the retinal proteomes from rats with OIR (n = 4) versus normal controls (n = 4). A total of 1325 proteins were quantified, and only one protein was removed due to lack of unique frames. The biological variation among retinas of each group was evaluated by measuring coefficients of variation (CVs) of protein intensities determined by ICB approach. The distributions of CV for the 1325 quantified proteins were found quite similar in controls and OIR subjects (Supplemental Figure 3). Box-and-whisker plots of CV distributions were calculated, where the bottom and the top of the boxes respectively correspond to the top 25th and 75th percentile values, the horizontal lines inside the box to the median CV values, and whiskers to the minimum and maximum values. The mean CV values for individual protein abundance values were 10.6% and 10.8%, respectively, for controls rats and these with OIR. The low variations of protein abundance values indicated the low biological variability within each group.

Differentially Expressed Proteins in Retinas of Controls versus OIR Rats

Quantitative investigations of the retinal proteomes in the rodent model of OIR, have been conducted using iTRAQ technique.[27,28] Zhou et al. employed iTRAQ and 2D nanoLC-nanoESI-MS/MS to compare the relative proteomic changes from control and OIR mice.[28] In that study a total of 264 protein groups were quantified, and 28 proteins were selected as altered proteins (≥1.2-fold change). The criteria of ≥1.2-fold change threshold and $p \leq 0.05$ were also used to determine altered proteins in 182 proteins that commonly identified in the

three iTRAQ retinal proteome analyses (P12 versus P12C, P17 versus P17C, and P12 versus P17) in a mouse model of OIR.[27] In the current study, due to the accurate and reliable quantification of ICB and the low level of false-positive in biomarker discovery,[22] we were able to apply a similar criteria of at least 1.3-fold change (ratio ≥1.30 or ≤0.77) and statistical *p*-values ≤0.05 to select significantly altered proteins, while quantifying more protein groups (1325).

Removal of mis-assigned frames is critical to warrant high-quality quantitative data, which is often caused by incorrect peptide identification and/or indistinguishable *m/z* and retention time of peaks. In order to reduce mis-assigned frames to protein ID, besides the critical criteria for peptide identification, we used a sum-of-intensity (SOI) method with outlier removal to determine protein ratio in this study. It has been reported that the SOI approach provides the most accurate estimates of true protein ratios of among MS1-based methods, and outlier rejection further improves the SOI approach when analyzing data from isotope-labeling experiment.[44] Our previous studies also employed the SOI method to calculate the protein ratio in ICB quantitation analysis.[22,26] In this study we used this biological data set to evaluate the improvement by sum-of-intensity with outlier rejection (SOI-R) over these without rejection.

Using the criteria of a fold change threshold of 1.3 and statistical *p*-values ≤0.05, 30 and 32 unique protein groups were determined as differentially expressed proteins with high confidence by SOI and SOI-R, respectively. The individual abundance values of 1325 proteins and associated peptide information in each retina are shown in Supplemental Table 2. Twenty-nine (93.5%) altered proteins were both determined by these two protein ratio estimation methods, and an excellent linear correlation ($R^2 = 0.97$) of protein ratios between the two methods was observed (Figure 3A). Radixin, determined as an altered protein by SOI method, was quantified by five unique peptides, but four (80%) of them have ratios around 1.0, as shown in Figure 3B. The outlier removal analysis made it possible to remove the outlier (red spots in Figure 3B) and resulted in a protein ratio that agrees well with the majority of peptide ratios. Further investigation revealed that the intensity (2.2×10^8) of this outlier is 9.2-fold higher than the mean intensity of remaining peptides ($(2.3 \pm 0.8) \times 10^7$) in radixin (Supplemental Figure 4). This outlier was likely either misidentified or from modified/truncated domain of the protein. Moreover, two other proteins, rootletin and craniofacial development protein 1 (Cfdp1), were determined by SOI-R as altered proteins but not by SOI for a similar reason (Figure 3B). All in all, SOI-R appears to provide a similar list of biomarker candidates with reduced false-positives/negatives comparing to SOI approach.

Out of the 32 altered proteins determined by SOI-R, 20 proteins were elevated, and 12 were decreased in retinas of OIR rats as shown in the volcano plots (fold-change vs *p*-values) (Figure 4). The black dashed lines denote the cutoff thresholds, while the altered proteins under these thresholds are indicated by red dots. A heat map plot of the intensities of altered proteins in the eight animals was further shown in Figure 5. As indicated in the tree diagrams, four OIR and four controls were classified into their own corresponding clusters as expected. Detailed information on the significantly altered proteins is shown in Table 1.

To further evaluate whether corresponding peptide ratios agree well with the protein ratios, the ratios of peptides from altered proteins were investigated. Out of the 96 unique quantifiable peptides assigned to the 20 elevated proteins, the majority of them (92, 95.8%) had an elevated expression ratio (Supplemental Figure 5). For a randomly selected example: ezrin, one of the elevated proteins (1.42-fold) was quantified with five unique peptides, and all of them had relative ratios >1.3 (range from 1.36 to 1.56). A similar trend was also observed in decreased proteins, e.g., 39 of the total of 42 peptides in these proteins had a decreased expression ratio (Supplemental Figure 5), indicating the good consistency between protein ratio and peptide ratio.

Functional Annotation and Validation of Proteins of High Interest

Our previous studies showed that retinal neovascularization occurs and higher blood O_2 and SO_2 levels are observed in P21 rats that have been exposed to constant hyperoxia (50% O_2) for 14 days and then RA for 7 days.[17] Here individual biological samples, instead of pooled samples as in previous work,[27,28] were used for investigation. More than 1300 unique protein groups were analyzed, and 32 proteins were determined to be altered in the OIR group compared to the control group as described above. Functional annotation was performed for these altered proteins and groups or individuals of high interest are further discussed in this section.

The 32 altered proteins were assigned to six major categories of biological processes on the basis of IPA and manual literature investigation. The six categories reflect key biological processes altered in the rat retinas suffering OIR (Supplemental Figure 6 and Table 1). The altered proteins in categories such as transport, visual system development and function, and inflammatory response were consistent with previous observations regarding ROP.[28,45] Moreover, elevated glial fibrillary acidic protein (GFAP) and decreased crystalline proteins in OIR retinas of mice models have been observed in previous studies.[27,28] The GFAP level in Müller cells was significantly increased in OIR P17 retinas compared with the control, especially in the distal branches of Müller cells.[27] In this study, GFAP, a sensitive marker for retinal degeneration and traumatic brain injury,[22,46] was increased 2.5-fold in OIR retinas of a rat model and validated by Western blot analysis (Figure 6). It is possible hypoxia also elicits elevation of GFAP in brain.[47] However, it is not likely the observed GFAP elevation was due to the increase of circulating GFAP consequent to elevation in brain, because of the very low circulating levels of GFAP following a cerebral hypoxia event[48,49] and the fact that blood was effectively removed from retina by perfusion and washing. Additionally, the elevated level of GFAP in retina agree well with observation in other OIR models.[27,28] Three β-crystalline proteins (A2, A3, and B2) were decreased in OIR retinas by ion-current-based quantification, consistent with previous observation by iTRAQ.[28] This indicates some mediators or pathways were shared in the process of retinal neovascularization of those different mouse or rat OIR models.

Previous studies show that hypoxia inducible factor (HIF)1-VEGF pathway is associated with the retinal neovascularization of ROP.[50–52] One angiogenesis-associated protein, 150 kDa oxygen-regulated protein, was previously identified as differentially expressed proteins in retinas of OIR.[27] In this study, altered proteins such as annexin A3 (ANXA3, elevated

3.4-fold), clusterin (elevated 1.8-fold), STAT1 (elevated 4.2-fold), ras-related protein Rab-21 (Rab21, elevated 1.4-fold), and moesin (elevated 1.3-fold) that associated with cell migration process, were also found to be involved in the HIF1-VEGF pathway. The network of proteins associated in this pathway is illustrated in Figure 7. The HIF1-VEGF associated network is closely related to OIR. For instance, ANXA3 is a member of calcium-binding protein family that bind membrane phospholipids in a calcium concentration-dependent manner.[53] It has been reported that ANXA3 could induce the transactivation activity of HIF-1 and lead to increase of VEGF secretion irrespective of oxygen level; thus, it is regarded as an angiogenic mediator for cancers.[54,55] In this study, ANXA3 is highly elevated in retinas of OIR as shown in Table 1, and may serve as a new therapeutic target for ROP. Clusterin, a glycoprotein also known as apolipoprotein J, could be expressed in Müller cells of the retina and is up-regulated in the retinal degeneration of rat models.[22,56,57] Protective effect of clusterin on blood-retinal barrier breakdown was also suggested in diabetic retinopathy.[58] Recent studies showed that nuclear clusterin transcription could be directly regulated by HIF-1α.[59] Our previous study showed that reactive oxygen species (ROS) such as H_2O_2 level in choroid of OIR is significantly higher ($p < 0.01$) than that in controls and may lead to high H_2O_2 level in retinas of OIR.[17] Thus, the elevated STAT1 here may play a similar role of response to intracellular ROS in retinas of OIR as these in human diseases.[60] The elevated STAT1 in OIR retinas of the rat model was further validated by immunoassay analysis (Figure 6). STAT1 may also play a role to negatively regulate VEGF through HIF1[61] and form a feedback loop (Figure 7). Another elevated protein Rab21 is important in Rho GTPase signaling, mediating recycling of integrin α5β1 for the activation of RhoA.[62] Direct activation of RhoA by ROS has been demonstrated.[63] The Rho-ROCK pathway is essential for VEGF-induced hyperpermeability[64] and also may play a similar role in retinas of OIR. VEGF-C activated RhoA/ROCK-2 pathway leads to upregulation and activation of moesin protein.[65] Moesin, one member of ezrin/radixin/moesin (ERM) proteins, was also observed to be elevated in retinas of OIR in this study, further indicating that the Rab21/RhoA/ROCK-2/moesin signaling pathway is involved in retinal neovascularization of OIR. Rho-kinase mediators may serve as therapeutic targets for the treatment of retinal neovascularization, as suggested previously.[66] In addition, Rho GTPases requires an essential downstream effector, STAT3, to regulate multiple cellular functions.[67]

The ERM proteins are linkers between plasma membrane proteins and the actin cytoskeleton, and they participate in diverse functions such as cell morphogenesis, endocytosis/exocytosis, adhesion, and migration.[68] In this study, increased expression of ezrin and moesin was observed for the first time in retinas of OIR. It has been reported that ezrin plays an important role in the morphogenesis of apical microvilli and basal infoldings of retinal pigment epithelial cells (RPE)[69] and recruits signaling molecules that regulate the activity of membrane proteins in response to external signals.[68] Recently, moesin was found to facilitate lipopolysaccharide (LPS) recognition and the subsequent expression of proinflammatory cytokines.[70] The expression and phosphorylation of moesin can be stimulated by LPS through directly binding to its carboxyl terminus.[70] LPS, an endotoxin of Gram-negative bacteria, could mimic the clinical scenario of chorioamnionitis in pregnant women and cause preterm birth in animals and humans.[71] In addition, a novel model of ROP

by systemic inflammation induced by postnatal LPS administration has been demonstrated recently.[72] Little is known about the association between the models of and LPS-induced ROP. Here, on the basis of the proteomics results, we speculate that moesin may be one of the key regulators that are important in both the processes of retinal neovascularization of the OIR models and LPS-induced ROP models. It may also provide new clues on the potential molecular mechanisms of anti-inflammatory drugs such as ketorolac, an inhibitor of LPS-induced inflammation,[73] which is capable of reducing the risk of developing severe ROP in preterm newborns without producing obvious undesirable side effects.[73]

CONCLUSIONS

The comprehensive proteomics studies of OIR models may substantially enhance our insights into the pathogenesis of ROP and might provide potential targets for therapeutic intervention,[1] despite that the animals in these models are not premature. Here we have performed a relatively extensive profiling of the proteomic changes in retinas of OIR rats using an ion-current-based MS1 approach. The quantification of >1300 proteins during retinal neovascularization and the discovery of many differentially altered proteins from retinas in OIR vs controls indicate that this approach is sensitive and extensive for proteomic profiling of the retinal proteome, which is rich in membrane proteins. Many altered proteins reflect various known complex processes of ROP such as inflammation response, abnormal visual development, and HIF1-VEGF pathway. Novel discoveries included changed proteins and pathways that were not previously known to be associated with ROP or OIR, such as STAT1, annexin A3, ERM, and Rab21/RhoA/ROCK2 signaling pathway, which may provide new insights in defining new therapeutic targets for ROP. Moreover, the results suggested that moesin-induced signaling may play an important role during the development of ROP in both LPS and OIR models. In conclusion, the ICB quantitative strategy is demonstrated to be a useful tool for exploring the pathological mechanisms of human diseases and to identify potential molecular and biochemical targets for interventions.

ACKNOWLEDGMENTS

This work was supported by a Center of Protein Therapeutics Consortium Award, by the NIH grants U54HD071594, AG048388, HL103411, and AI060260, and by the American Heart Association award 12SDG9450036.

ABBREVIATIONS

AUC	area-under-the-curve
CV	coefficient of variation
emPAI	exponentially modified protein abundance index
ERM	ezrin/radixin/moesin
FDR	false discovery rate
GAPDH	glyceraldehyde-3-phosphate dehydrogenase
GFAP	glial fibrillary acidic protein

GO	gene ontology
H_2O_2	hydrogen peroxide
HIF1	hypoxia inducible factor 1
ICB	ion-current-based MS1 quantification
IPA	ingenuity pathway analysis
iTRAQ	isobaric tags for relative and absolute quantification
LC-MS	liquid chromatography–mass spectrometry
LPS	lipopolysaccharide
MS2-TIC	MS2-total ion-current
NSAF	normalized spectral abundance factor
OIR	oxygen-induced retinopathy
RA	room air
ROP	retinopathy of prematurity
ROS	reactive oxygen species
RPE	retinal pigment epithelial cells
SOI	sum of intensity
SOI-R	sum of intensity with outlier rejection
SpC	spectral counting
STAT1	signal transducer and activator of transcription 1
VEGF	vascular endothelial growth factor

REFERENCES

(1). Hartnett ME, Penn JS. Mechanisms and management of retinopathy of prematurity. N. Engl. J. Med. 2013; 368:1162–1163. [PubMed: 23514302]

(2). Smith LE, Hard AL, Hellstrom A. The biology of retinopathy of prematurity: how knowledge of pathogenesis guides treatment. Clin. Perinatol. 2013; 40:201–214. [PubMed: 23719305]

(3). Smith LE. Pathogenesis of retinopathy of prematurity. Growth Horm. IGF Res. 2004; 14(Suppl.A):S140–144.

(4). Flynn JT. Acute proliferative retrolental fibroplasia: multivariate risk analysis. Trans. Am. Ophthalmol. Soc. 1983; 81:549–591. [PubMed: 6689564]

(5). Fierson WM. Screening examination of premature infants for retinopathy of prematurity. Pediatrics. 2013; 131:189–195. [PubMed: 23277315]

(6). Ng EY, Connolly BP, McNamara JA, Regillo CD, Vander JF, Tasman WA. comparison of laser photocoagulation with cryotherapy for threshold retinopathy of prematurity at 10 years: part 1. Visual function and structural outcome. Ophthalmology. 2002; 109:928–934. discussion 935. [PubMed: 11986099]

(7). McCollum GW, Rajaratnam VS, Bullard LE, Yang R, Penn JS. Herbimycin A inhibits angiogenic activity in endothelial cells and reduces neovascularization in a rat model of retinopathy of prematurity. Exp. Eye Res. 2004; 78:987–995. [PubMed: 15051479]

(8). Drixler TA, Borel Rinkes IH, Ritchie ED, Treffers FW, van Vroonhoven TJ, Gebbink MF, Voest EE. Angiostatin inhibits pathological but not physiological retinal angiogenesis. Invest. Ophthalmol. Vis. Sci. 2001; 42:3325–3330. [PubMed: 11726640]

(9). Smith LE, Shen W, Perruzzi C, Soker S, Kinose F, Xu X, Robinson G, Driver S, Bischoff J, Zhang B, Schaeffer JM, Senger DR. Regulation of vascular endothelial growth factor-dependent retinal neovascularization by insulin-like growth factor-1 receptor. Nat. Med. 1999; 5:1390–1395. [PubMed: 10581081]

(10). Smith LE, Wesolowski E, McLellan A, Kostyk SK, D'Amato R, Sullivan R, D'Amore PA. Oxygen-induced retinopathy in the mouse. Invest. Ophthalmol. Vis. Sci. 1994; 35:101–111. [PubMed: 7507904]

(11). Stahl A, Connor KM, Sapieha P, Chen J, Dennison RJ, Krah NM, Seaward MR, Willett KL, Aderman CM, Guerin KI, Hua J, Lofqvist C, Hellstrom A, Smith LE. The mouse retina as an angiogenesis model. Invest. Ophthalmol. Vis Sci. 2010; 51:2813–2826. [PubMed: 20484600]

(12). Brock RS, Gebrekristos BH, Kuniyoshi KM, Modanlou HD, Falcao MC, Beharry KD. Biomolecular effects of JB1 (an IGF-I peptide analog) in a rat model of oxygen-induced retinopathy. Pediatr. Res. 2011; 69:135–141. [PubMed: 21057375]

(13). Cringle SJ, Yu DY. A multi-layer model of retinal oxygen supply and consumption helps explain the muted rise in inner retinal PO(2) during systemic hyperoxia. Comp. Biochem. Physiol. A: Mol. Integr. Physiol. 2002; 132:61–66. [PubMed: 12062192]

(14). Penn JS, Tolman BL, Lowery LA. Variable oxygen exposure causes preretinal neovascularization in the newborn rat. Invest. Ophthalmol. Vis. Sci. 1993; 34:576–585. [PubMed: 8449677]

(15). Stone J, Chan-Ling T, Pe'er J, Itin A, Gnessin H, Keshet E. Roles of vascular endothelial growth factor and astrocyte degeneration in the genesis of retinopathy of prematurity. Invest. Ophthalmol. Vis. Sci. 1996; 37:290–299. [PubMed: 8603833]

(16). Stone J, Itin A, Alon T, Pe'er J, Gnessin H, Chan-Ling T, Keshet E. Development of retinal vasculature is mediated by hypoxia-induced vascular endothelial growth factor (VEGF) expression by neuroglia. J. Neurosci. 1995; 15:4738–4747. [PubMed: 7623107]

(17). Beharry KD, Cai CL, Sharma P, Bronshtein V, Valencia GB, Lazzaro DR, Aranda JV. Hydrogen peroxide accumulation in the choroid during intermittent hypoxia increases risk of severe oxygen-induced retinopathy in neonatal rats. Invest. Ophthalmol. Vis. Sci. 2013; 54:7644–7657. [PubMed: 24168990]

(18). Mueller LN, Brusniak MY, Mani DR, Aebersold R. An assessment of software solutions for the analysis of mass spectrometry based quantitative proteomics data. J. Proteome Res. 2008; 7:51–61. [PubMed: 18173218]

(19). Bantscheff M, Schirle M, Sweetman G, Rick J, Kuster B. Quantitative mass spectrometry in proteomics: a critical review. Anal. Bioanal. Chem. 2007; 389:1017–1031. [PubMed: 17668192]

(20). Neilson KA, Ali NA, Muralidharan S, Mirzaei M, Mariani M, Assadourian G, Lee A, van Sluyter SC, Haynes PA. Less label, more free: approaches in label-free quantitative mass spectrometry. Proteomics. 2011; 11:535–553. [PubMed: 21243637]

(21). Nouri-Nigjeh E, Sukumaran S, Tu C, Li J, Shen X, Duan X, DuBois DC, Almon RR, Jusko WJ, Qu J. Highly multiplexed and reproducible ion-current-based strategy for large-scale quantitative proteomics and the application to protein expression dynamics induced by methylprednisolone in 60 rats. Anal. Chem. 2014; 86:8149–8157. [PubMed: 25072516]

(22). Tu C, Li J, Jiang X, Sheflin LG, Pfeffer BA, Behringer M, Fliesler SJ, Qu J. Ion-current-based proteomic profiling of the retina in a rat model of Smith-Lemli-Opitz syndrome. Mol. Cell Proteomics. 2013; 12:3583–3598. [PubMed: 23979708]

(23). Gautier V, Mouton-Barbosa E, Bouyssie D, Delcourt N, Beau M, Girard JP, Cayrol C, Burlet-Schiltz O, Monsarrat B, Gonzalez de Peredo A. Label-free quantification and shotgun analysis of complex proteomes by one-dimensional SDS-PAGE/NanoLC-MS: evaluation for the large scale analysis of inflammatory human endothelial cells. Mol. Cell Proteomics. 2012; 11:527–539. [PubMed: 22518033]

(24). Theron L, Gueugneau M, Coudy C, Viala D, Bijlsma A, Butler-Browne G, Maier A, Bechet D, Chambon C. Label-free quantitative protein profiling of vastus lateralis muscle during human aging. Mol. Cell Proteomics. 2014; 13:283–294. [PubMed: 24217021]

(25). Qu J, Young R, Page BJ, Shen X, Tata N, Li J, Duan X, Fallavollita JA, Canty JM Jr. Reproducible ion-current-based approach for 24-plex comparison of the tissue proteomes of hibernating versus normal myocardium in swine models. J. Proteome Res. 2014; 13:2571–2584. [PubMed: 24697261]

(26). Tu C, Li J, Sheng Q, Zhang M, Qu J. Systematic Assessment of Survey Scan and MS2-Based Abundance Strategies for Label-Free Quantitative Proteomics Using High-Resolution MS Data. J. Proteome Res. 2014; 13:2069–2079. [PubMed: 24635752]

(27). Kim SJ, Jin J, Kim YJ, Kim Y, Yu HG. Retinal proteome analysis in a mouse model of oxygen-induced retinopathy. J. Proteome Res. 2012; 11:5186–5203. [PubMed: 23039900]

(28). Zhou L, X L, Koh SK, Xiaorong L, Beuerman RW. Quantitative proteomic analysis of retina in oxygen-induced retinopathy mice using iTRAQ with 2D NanoLC-nanoESI-MS/MS. JIOMICS. 2011; 1:226–235.

(29). Coleman RJ, Beharry KD, Brock RS, Abad-Santos P, Abad-Santos M, Modanlou HD. Effects of brief, clustered versus dispersed hypoxic episodes on systemic and ocular growth factors in a rat model of oxygen-induced retinopathy. Pediatr. Res. 2008; 64:50–55. [PubMed: 18344903]

(30). Duan X, Young R, Straubinger RM, Page B, Cao J, Wang H, Yu H, Canty JM, Qu J. A straightforward and highly efficient precipitation/on-pellet digestion procedure coupled with a long gradient nano-LC separation and Orbitrap mass spectrometry for label-free expression profiling of the swine heart mitochondrial proteome. J. Proteome Res. 2009; 8:2838–2850. [PubMed: 19290621]

(31). Elias JE, Haas W, Faherty BK, Gygi SP. Comparative evaluation of mass spectrometry platforms used in large-scale proteomics investigations. Nat. Methods. 2005; 2:667–675. [PubMed: 16118637]

(32). Searle BC. Scaffold: a bioinformatic tool for validating MS/MS-based proteomic studies. Proteomics. 2010; 10:1265–1269. [PubMed: 20077414]

(33). Lopez MF, Kuppusamy R, Sarracino DA, Prakash A, Athanas M, Krastins B, Rezai T, Sutton JN, Peterman S, Nicolaides K. Mass spectrometric discovery and selective reaction monitoring (SRM) of putative protein biomarker candidates in first trimester Trisomy 21 maternal serum. J. Proteome Res. 2011; 10:133–142. [PubMed: 20499897]

(34). Tu C, Sheng Q, Li J, Shen X, Zhang M, Shyr Y, Qu J. ICan: An Optimized Ion-Current-Based Quantification Procedure with Enhanced Quantitative Accuracy and Sensitivity in Biomarker Discovery. J. Proteome Res. 2014; 13:5888–5897. [PubMed: 25285707]

(35). Grubbs FE. Sample Criteria for Testing Outlying Observations. Ann. Math. Statist. 1950; 21:27–58.

(36). Grossmann J, Roschitzki B, Panse C, Fortes C, Barkow-Oesterreicher S, Rutishauser D, Schlapbach R. Implementation and evaluation of relative and absolute quantification in shotgun proteomics with label-free methods. J. Proteomics. 2010; 73:1740–1746. [PubMed: 20576481]

(37). Ishihama Y, Oda Y, Tabata T, Sato T, Nagasu T, Rappsilber J, Mann M. Exponentially modified protein abundance index (emPAI) for estimation of absolute protein amount in proteomics by the number of sequenced peptides per protein. Mol. Cell Proteomics. 2005; 4:1265–1272. [PubMed: 15958392]

(38). Zhang Y, Wen Z, Washburn MP, Florens L. Refinements to label free proteome quantitation: how to deal with peptides shared by multiple proteins. Anal. Chem. 2010; 82:2272–2281. [PubMed: 20166708]

(39). Huang da W, Sherman BT, Lempicki RA. Systematic and integrative analysis of large gene lists using DAVID bioinformatics resources. Nat. Protoc. 2009; 4:44–57. [PubMed: 19131956]

(40). de Hoon MJ, Imoto S, Nolan J, Miyano S. Open source clustering software. Bioinformatics. 2004; 20:1453–1454. [PubMed: 14871861]

(41). Penn JS, Henry MM, Tolman BL. Exposure to alternating hypoxia and hyperoxia causes severe proliferative retinopathy in the newborn rat. Pediatr. Res. 1994; 36:724–731. [PubMed: 7898981]

(42). McIlwain S, Mathews M, Bereman MS, Rubel EW, MacCoss MJ, Noble WS. Estimating relative abundances of proteins from shotgun proteomics data. BMC Bioinformatics. 2012; 13:308. [PubMed: 23164367]

(43). Griffin NM, Yu J, Long F, Oh P, Shore S, Li Y, Koziol JA, Schnitzer JE. Label-free, normalized quantification of complex mass spectrometry data for proteomic analysis. Nat. Biotechnol. 2010; 28:83–89. [PubMed: 20010810]

(44). Carrillo B, Yanofsky C, Laboissiere S, Nadon R, Kearney RE. Methods for combining peptide intensities to estimate relative protein abundance. Bioinformatics. 2010; 26:98–103. [PubMed: 19892804]

(45). Sood BG, Madan A, Saha S, Schendel D, Thorsen P, Skogstrand K, Hougaard D, Shankaran S, Carlo W. Perinatal systemic inflammatory response syndrome and retinopathy of prematurity. Pediatr. Res. 2010; 67:394–400. [PubMed: 20032809]

(46). Lumpkins KM, Bochicchio GV, Keledjian K, Simard JM, McCunn M, Scalea T. Glial fibrillary acidic protein is highly correlated with brain injury. J. Trauma. 2008; 65:778–782. discussion 782–774. [PubMed: 18849790]

(47). Burtrum D, Silverstein FS. Hypoxic-ischemic brain injury stimulates glial fibrillary acidic protein mRNA and protein expression in neonatal rats. Exp. Neurol. 1994; 126:112–118. [PubMed: 8157121]

(48). Hayes RL, Mondello S, Wang K. Glial fibrillary acidic protein: a promising biomarker in pediatric brain injury. Pediatr. Crit. Care Med. 2011; 12:603–604. [PubMed: 21897166]

(49). Bembea MM, Savage W, Strouse JJ, Schwartz JM, Graham E, Thompson CB, Everett A. Glial fibrillary acidic protein as a brain injury biomarker in children undergoing extracorporeal membrane oxygenation. Pediatr. Crit. Care Med. 2011; 12:572–579. [PubMed: 21057367]

(50). Hartnett ME. Pathophysiology and Mechanisms of Severe Retinopathy of Prematurity. Ophthalmology. 2015; 122:200–210. [PubMed: 25444347]

(51). Park SW, Kim JH, Kim KE, Jeong MH, Park H, Park B, Suh YG, Park WJ. Beta-lapachone inhibits pathological retinal neovascularization in oxygen-induced retinopathy via regulation of HIF-1alpha. J. Cell Mol. Med. 2014; 18:875–884. [PubMed: 24533641]

(52). Sapieha P, Joyal JS, Rivera JC, Kermorvant-Duchemin E, Sennlaub F, Hardy P, Lachapelle P, Chemtob S. Retinopathy of prematurity: understanding ischemic retinal vasculopathies at an extreme of life. J. Clin. Invest. 2010; 120:3022–3032. [PubMed: 20811158]

(53). Raynal P, Pollard HB. Annexins: the problem of assessing the biological role for a gene family of multifunctional calcium- and phospholipid-binding proteins. Biochim. Biophys. Acta. 1994; 1197:63–93. [PubMed: 8155692]

(54). Wu N, Liu S, Guo C, Hou Z, Sun MZ. The role of annexin A3 playing in cancers. Clin. Transl. Oncol. 2013; 15:106–110. [PubMed: 23011854]

(55). Park JE, Lee DH, Lee JA, Park SG, Kim NS, Park BC, Cho S. Annexin A3 is a potential angiogenic mediator. Biochem. Biophys. Res. Commun. 2005; 337:1283–1287. [PubMed: 16236264]

(56). Gwon JS, Kim IB, Lee MY, Oh SJ, Chun MH. Expression of clusterin in Muller cells of the rat retina after pressure-induced ischemia. Glia. 2004; 47:35–45. [PubMed: 15139011]

(57). Wong P, Ulyanova T, Organisciak DT, Bennett S, Lakins J, Arnold JM, Kutty RK, Tenniswood M, vanVeen T, Darrow RM, Chader G. Expression of multiple forms of clusterin during light-induced retinal degeneration. Curr. Eye Res. 2001; 23:157–165. [PubMed: 11803476]

(58). Kim JH, Yu YS, Min BH, Kim KW. Protective effect of clusterin on blood-retinal barrier breakdown in diabetic retinopathy. Invest. Ophthalmol. Vis. Sci. 2010; 51:1659–1665. [PubMed: 19875648]

(59). Park J, Park SY, Shin E, Lee SH, Kim YS, Lee DH, Roh GS, Kim HJ, Kang SS, Cho GJ, Jeong BY, Kim H, Choi WS. Hypoxia inducible factor-1alpha directly regulates nuclear clusterin transcription by interacting with hypoxia response elements in the clusterin promoter. Mol. Cells. 2014; 37:178–186. [PubMed: 24599003]

(60). Simon AR, Rai U, Fanburg BL, Cochran BH. Activation of the JAK-STAT pathway by reactive oxygen species. Am. J. Physiol. 1998; 275:C1640–1652. [PubMed: 9843726]

(61). Albasanz-Puig A, Murray J, Namekata M, Wijelath ES. Opposing roles of STAT-1 and STAT-3 in regulating vascular endothelial growth factor expression in vascular smooth muscle cells. Biochem. Biophys. Res. Commun. 2012; 428:179–184. [PubMed: 23068100]

(62). Pellinen T, Tuomi S, Arjonen A, Wolf M, Edgren H, Meyer H, Grosse R, Kitzing T, Rantala JK, Kallioniemi O, Fassler R, Kallio M, Ivaska J. Integrin trafficking regulated by Rab21 is necessary for cytokinesis. Dev. Cell. 2008; 15:371–385. [PubMed: 18804435]

(63). Aghajanian A, Wittchen ES, Campbell SL, Burridge K. Direct activation of RhoA by reactive oxygen species requires a redox-sensitive motif. PLoS One. 2009; 4:e8045. [PubMed: 19956681]

(64). Sun H, Breslin JW, Zhu J, Yuan SY, Wu MH. Rho and ROCK signaling in VEGF-induced microvascular endothelial hyperpermeability. Microcirculation. 2006; 13:237–247. [PubMed: 16627366]

(65). He M, Cheng Y, Li W, Liu Q, Liu J, Huang J, Fu X. Vascular endothelial growth factor C promotes cervical cancer metastasis via up-regulation and activation of RhoA/ROCK-2/moesin cascade. BMC Cancer. 2010; 10:170. [PubMed: 20429915]

(66). Fang X, Ueno M, Yamashita T, Ikuno Y. RhoA activation and effect of Rho-kinase inhibitor in the development of retinal neovascularization in a mouse model of oxygen-induced retinopathy. Curr. Eye Res. 2011; 36:1028–1036. [PubMed: 21999228]

(67). Debidda M, Wang L, Zang H, Poli V, Zheng Y. A role of STAT3 in Rho GTPase-regulated cell migration and proliferation. J. Biol. Chem. 2005; 280:17275–17285. [PubMed: 15705584]

(68). Arpin M, Chirivino D, Naba A. Zwaenepoel, I. Emerging role for ERM proteins in cell adhesion and migration. Cell Adh. Migr. 2011; 5:199–206. [PubMed: 21343695]

(69). Bonilha VL, Finnemann SC, Rodriguez-Boulan E. Ezrin promotes morphogenesis of apical microvilli and basal infoldings in retinal pigment epithelium. J. Cell Biol. 1999; 147:1533–1548. [PubMed: 10613910]

(70). Iontcheva I, Amar S, Zawawi KH, Kantarci A, Van Dyke TE. Role for moesin in lipopolysaccharide-stimulated signal transduction. Infect. Immun. 2004; 72:2312–2320. [PubMed: 15039356]

(71). Martinez-Lopez DG, Funderburg NT, Cerissi A, Rifaie R, Aviles-Medina L, Llorens-Bonilla BJ, Sleasman J, Luciano AA. Lipopolysaccharide and soluble CD14 in cord blood plasma are associated with prematurity and chorioamnionitis. Pediatr. Res. 2014; 75:67–74. [PubMed: 24135785]

(72). Hong HK, Lee HJ, Ko JH, Park JH, Park JY, Choi CW, Yoon C-H, Ahn SJ, Park KH, Woo SJ, Oh JY. Neonatal systemic inflammation in rats alters retinal vessel development and simulates pathologic features of retinopathy of prematurity. J. Neuroinflammation. 2014; 11:87. [PubMed: 24886524]

(73). Waterbury LD, Galindo D, Villanueva L, Nguyen C, Patel M, Borbridge L, Attar M, Schiffman RM, Hollander DA. Ocular penetration and anti-inflammatory activity of ketorolac 0.45% and bromfenac 0.09% against lipopolysaccharide-induced inflammation. J. Ocul. Pharmacol. Ther. 2011; 27:173–178. [PubMed: 21351868]

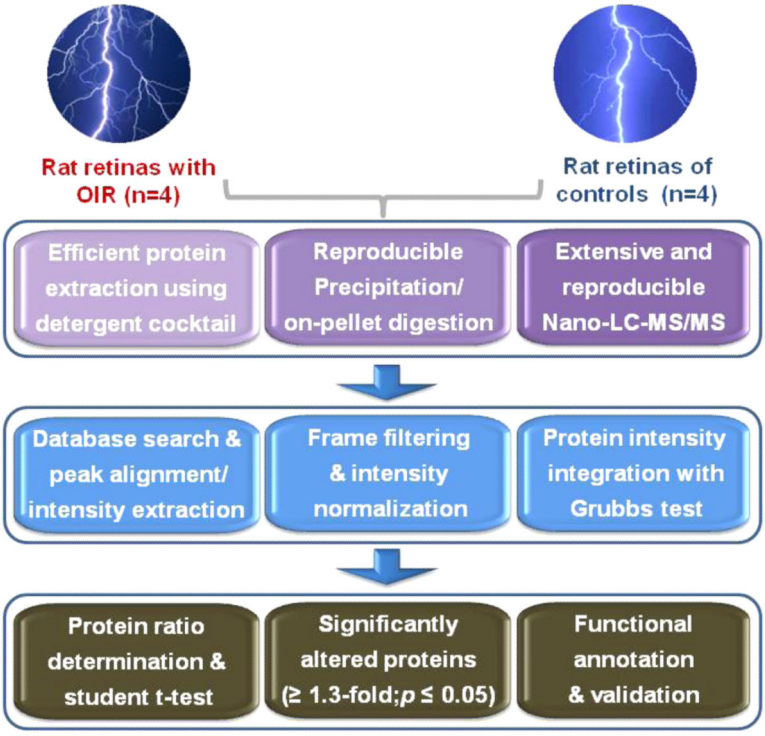

Figure 1.

Flowchart of the ion-current-based quantitation strategy applied for analyzing retinas from a rat model of oxygen-induced retinopathy (OIR) vs age-matched controls (n = 4 animals per group).

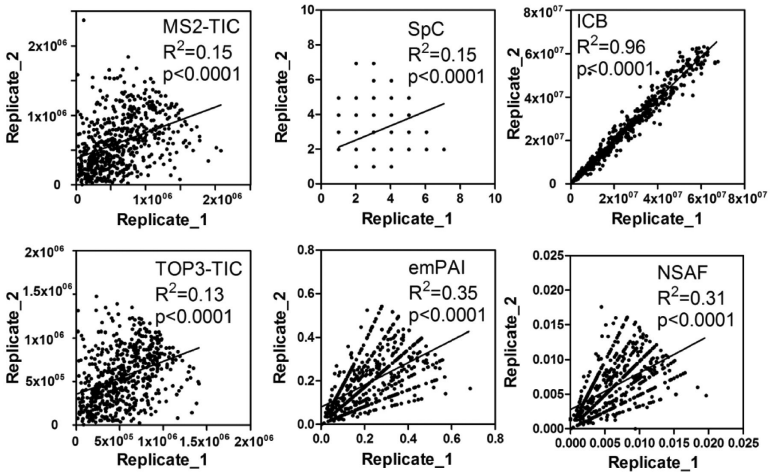

Figure 2.

Evaluation of reproducibility of protein abundance values for proteins of the lower 50% in abundance between technical replicates using different label-free approaches.

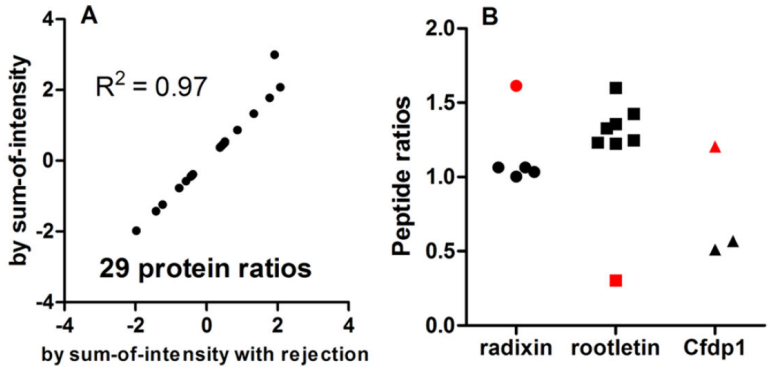

Figure 3.

Comparison between sum-of-intensity (SOI) and sum-of-intensity with rejection analysis (SOI-R) for protein ratio estimation. (A) Linear correlation of protein ratios determined by SOI and SOI-R. (B) Distribution of peptide ratios of radixin, rootletin, and Cfdp 1 that had quite different protein ratios by SOI and SOI-R analyses. The peptide outliers (red spots) were identified by Grubbs's test and therefore removed from consideration by SOI-R.

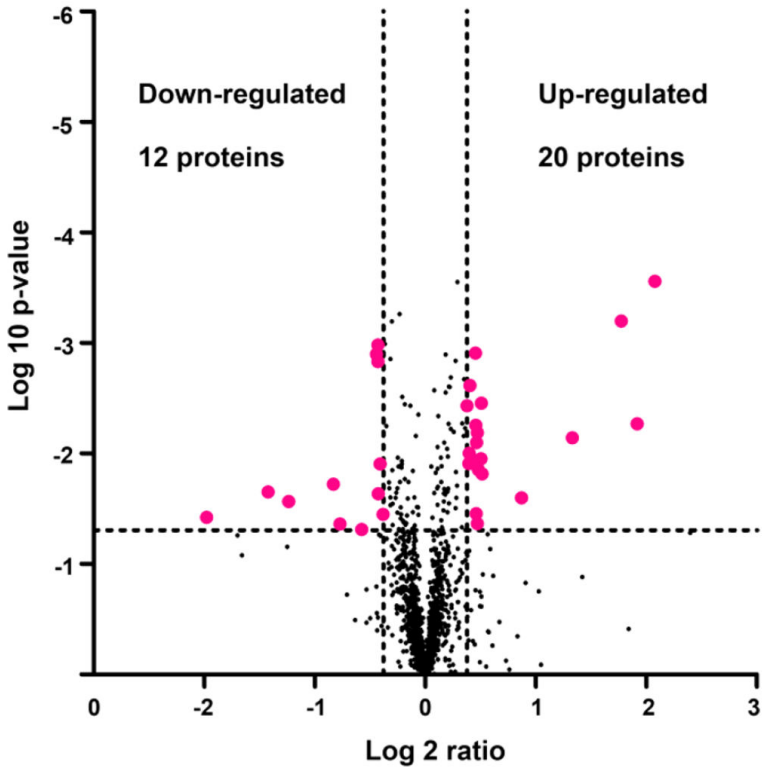

Figure 4.

Volcano plots illustrating the discovery of significantly altered proteins from OIR/control sample set using ICB approach. The *X*-axis shows the protein abundance ratios of individual proteins in OIR vs. control group, while the *Y*-axis shows the *p*-values (by Student's *t*-test statistics) for the comparison. Each dot represents a unique protein group, and the dashed lines denote the optimized cutoff thresholds ($p \leq 0.05$ and ≥1.3-fold change) that define significantly altered proteins, which are shown as red dots.

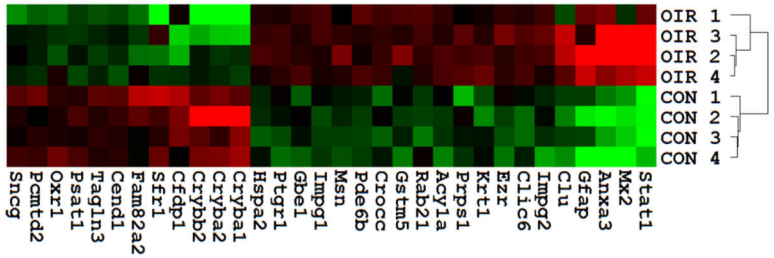

Figure 5.

Hierarchical clustering analysis of the 32 differentially expressed proteins observed in retinas from OIR rats (n = 4, OIR 1–OIR 4) vs controls (n = 4, CON 1–CON 4). The elevated protein intensities are shown in red, and the decreased protein intensities are shown in green.

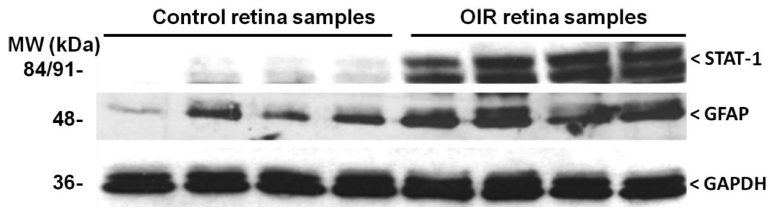

Figure 6.

Figure 6. Western blot analysis (anti-Stat1, anti-GFAP) demonstrates increased expression of Stat1 and GFAP in retinas of OIR rats (right panel, lanes 5–8) compared to retinas from age-matched control rats (left panel, lanes 1–4). GAPDH was used as loading control.

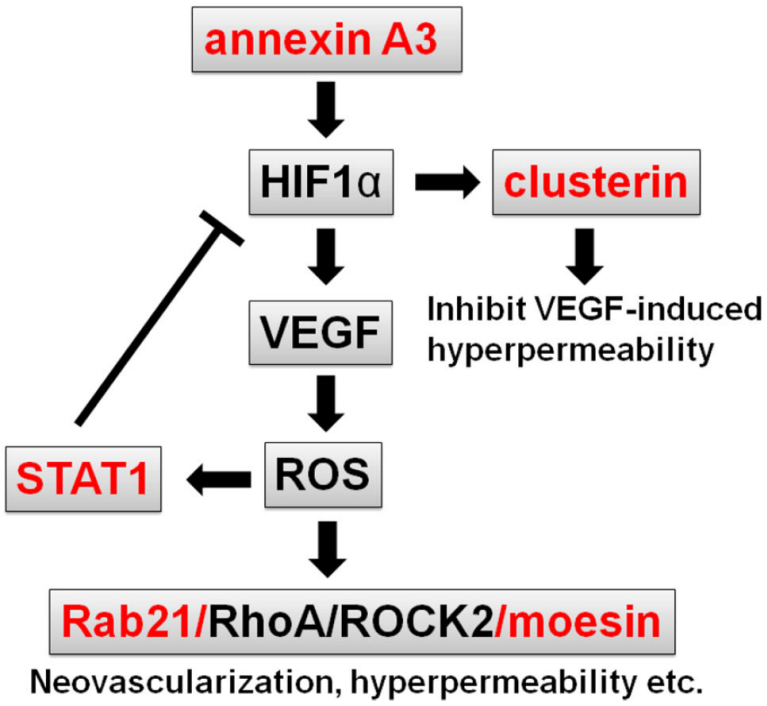

Figure 7.

Network of HIF1-VEGF pathway associated alterations observed in retinas of OIR rats (adapted from ref 1). Elevated proteins observed in this study are indicated in red.

Table 1

Significantly Altered Proteins in Retinas of a Rat Model of OIR (n = 4) versus Controls (n = 4) by the Ion-Current-Based Quantitation Analysis

accession no.	gene name	protein name	no. quantified peptides	ratio (COPD/normal)	standard deviation	p-value	biological process
P42225	Stat1	signal transducer and activator of transcription 1	2	4.22	1.47	<0.01	visual system develo inflammatory respon migration; transport;
P18589	Mx2	interferon-induced GTP-binding protein Mx2	9	3.78	1.78	<0.01	lipid metabolism; inflammatory respon
P14669	Anxa3	annexin A3	3	3.42	0.96	<0.01	inflammatory respon migration
P47819	Gfap	glial fibrillary acidic protein	11	2.52	0.84	<0.01	inflammatory respon migration
P05371	Clu	clusterin	5	1.83	0.58	0.03	lipid metabolism; inflammatory respon migration; transport;
P70628	Impg2	interphotoreceptor matrix proteoglycan 2	5	1.43	0.13	0.02	visual system develo
Q811Q2	Clic6	chloride intracellular channel protein 6	10	1.42	0.08	<0.01	transport
P31977	Ezr	ezrin	5	1.42	0.17	0.01	cell migration; transp apoptosis
Q6IMF3	Krt1	keratin, type II cytoskeletal 1	3	1.40	0.15	0.01	inflammatory respon cytoskeleton organiz
P60892	Prps1	ribose-phosphate pyrophospho kinase 1	3	1.39	0.14	0.04	carbohydrate metabo process; apoptosis
Q6AYS7	Acyla	aminoacylase-1A	2	1.39	0.08	<0.01	cellular amino acid m process
Q9Z1B2	Gstm5	glutathione *S*-transferase Mu 5	3	1.38	0.25	0.04	metabolic process
Q6AXT5	Rab21	Ras-related protein Rab-21	3	1.38	0.08	<0.01	cell migration
Q8CJ40	Crocc	rootletin	7	1.37	0.03	<0.01	cytoskeleton organiz
P23440	Pde6b	rod cGMP-specific 3′,5′-cyclic phosphodiesterase subunit β	8	1.37	0.14	<0.01	visual system develo
O35763	Msn	moesin	4	1.35	0.20	0.01	lipid metabolism; inflammatory respon migration; transport;
Q9ET62	Impg1	interphotoreceptor matrix proteoglycan 1	6	1.32	0.09	<0.01	visual system develo
Q9D6Y9	Gbel	1,4-α-glucan-branching enzyme	3	1.32	0.07	0.01	carbohydrate metabo
P97584	Ptgr1	prostaglandin reductase 1	2	1.31	0.06	0.01	lipid metabolism
P14659	Hspa2	heat shock-related 70 kDa protein 2	2	1.30	0.09	<0.01	response to stress; ap
P14881	Cryba1	β-crystallin A3	2	0.25	0.14	0.04	visual system develo
Q9JJV1	Cryba2	β-crystallin A2	3	0.37	0.15	0.02	visual system develo
P62697	Crybb2	β-crystallin B2	9	0.43	0.18	0.03	visual system develo
Q75UQ2	Cfdpl	craniofacial development protein 1	2	0.56	0.17	0.02	antiapoptosis
Q6TXG9	Sfr1	Swi5-dependent recombination DNA repair protein 1 homologue	2	0.59	0.22	0.04	unknown
Q66H15	Fam82a2	regulator of microtubule dynamics protein 3	2	0.67	0.12	0.05	apoptosis

accession no.	gene name	protein name	no. quantified peptides	ratio (COPD/normal)	standard deviation	*p*-value	biological process
Q5FVI4	Cend1	cell cycle exit and neuronal differentiation protein 1	4	0.74	0.06	<0.01	cytoskeleton organiz
Q99K85	Psat1	phosphoserine aminotransferase	2	0.74	0.05	<0.01	organic acid metabol
P37805	Tagln3	transgelin-3	6	0.74	0.05	<0.01	muscle organ develo
Q4V8B0	Oxr1	oxidation resistance protein 1	3	0.74	0.13	0.02	inflammatory respon
Q8BHD8	Pcmtd2	protein L-isoaspartate *O*-methyl transferase domain-containing protein 2	3	0.75	0.07	0.01	protein modification
Q63544	Sncg	γ-synuclein	4	0.77	0.13	0.04	transport; lipid metal